

Cite this: DOI: 10.1039/c9dt04571f

Permanent porosity and role of sulfonate groups in coordination networks constructed from a new polyfunctional phosphonato-sulfonate linker molecule†

Stephan Wöhlbrandt,^a Angela Igeska,^a Erik Svensson Grape,^{id}^b
Sigurd Øien-Ødegaard,^c A. Ken Inge ^{id}^b and Norbert Stock ^{id}^{*a}

The new linker molecule (H₂O₃PCH₂)₂N-CH₂C₆H₄SO₃H, (4-([bis(phosphonomethyl)amino)methyl]benzene-sulfonic acid, H₅L), bearing both phosphonic and sulfonic acid groups, was employed for the synthesis of new coordination polymers (CPs). Four new CPs of composition [Mg(H₃L)(H₂O)₂]-H₂O (**1**), [Mg₂(HL)(H₂O)₆]-2H₂O (**2**), [Ba(H₃L)(H₂O)]-H₂O (**3**) and [Pb₂(HL)]-H₂O (**4**), were discovered using high-throughput methods and all structures were determined by single-crystal X-ray diffraction (SCXRD). With increasing ionic radius of the metal ion, an increase in coordination number from CN = 6 (Mg²⁺) to CN = 9 (Ba²⁺) and an increase in the dimensionality of the network from 1D to 3D is observed. This is reflected in the composition of the IBU and the number of metal ions that are connected by each linker molecule, *i.e.* from three in **1** to ten in **4**. The connection of the IBUs leads to 1D and 2D structures in **1** and **2** with non-coordinating sulfonate groups, while **3** and **4** crystallise in MOF-type structures and coordination of the sulfonate groups is observed. The compounds exhibit thermal stabilities between 200 (**2**) and 345 °C (**4**) as proven by variable temperature powder X-ray diffraction (VT-PXRD) measurements. Title compound **4** contains micropores of 4 × 2 Å and reversible H₂O uptake of 50 mg g⁻¹ was demonstrated by vapour sorption measurements, making it the first porous metal phosphonosulfonate. Detailed characterisation, *i.e.* CHNS and TG analysis as well as NMR and IR spectroscopy measurements confirm the phase purity of the title compounds.

Received 28th November 2019,
Accepted 6th February 2020

DOI: 10.1039/c9dt04571f

rsc.li/dalton

1. Introduction

The field of metal organophosphonates is a diverse and ever-growing field of research.^{1–3} Most of the compounds are coordination polymers (CPs) featuring inorganic building units (IBUs) which can occur as isolated MO_x polyhedra in the structure, but also as dimers (M₂O_x), chains or layers.⁴ These IBUs are connected *via* organic linker molecules into crystalline networks, each with unique properties.^{5,6} The number of theoretical combinations is virtually limitless since for the synthesis only an organic linker molecule with a phosphonic acid

function and a suitable metal salt is needed. This variability results in compounds with various magnetic, luminescent, ion-exchange and proton-conducting properties.⁷ Furthermore, metal phosphonates were among the first porous coordination polymers,⁸ a field that is nowadays dominated by metal carboxylates.⁹ Nevertheless, recently important contributions to the field of porous metal phosphonates have been reported by various groups.^{1,3}

The introduction of additional functionalities to the organic linker, like amino, fluoro, methyl, or carboxylic groups, was carried out to study their influence on the formation of crystalline metal phosphonates. Many beautiful yet complex crystal structures were reported ranging from 0D-complexes to 2D-layered networks and 3D-connected porous frameworks.¹⁰

Organic linker molecules containing alkylamine groups have also been extensively used as starting materials for the synthesis of metal organophosphonates,¹¹ since the amino group can be straightforwardly converted into bis(phosphonomethyl)-amine groups ((H₂O₃PCH₂)₂N-). A dominant structural motif in these compounds are inorganic layers comprised

^aInstitut für Anorganische Chemie, Christian-Albrechts-Universität zu Kiel, 24098 Kiel, Germany. E-mail: stock@ac.uni-kiel.de

^bDepartment of Materials and Environmental Chemistry, Stockholm University, Stockholm 10691, Sweden

^cDepartment of Chemistry, University of Oslo, P.O. Box 1033, N-0315 Oslo, Norway

† Electronic supplementary information (ESI) available: PXRD patterns, crystallographic data, ¹H NMR and IR spectroscopy, TGA and sorption data, CHNS analysis. CCDC 1968802–1968805. For ESI and crystallographic data in CIF or other electronic format see DOI: 10.1039/c9dt04571f

of alternating MO_x polyhedra and phosphonate groups, which are separated by the organic part of the linker molecule, thus forming a hydrophobic region. The polarity of this region can be modified through the introduction of additional functional groups, such as $-\text{CH}_3$, $-\text{F}$ and $-\text{COOH}$. Especially the addition of $-\text{COOH}$ groups proved to be interesting due to a possible interconnection of the layers and extended hydrogen bonding. This concept can be taken further through the addition of a sulfonic acid function, which has previously not been introduced into the chemistry of the arylbis(phosphonomethyl)-amines.

Here we report our results on the incorporation of a sulfonic acid function into a linker molecule containing a $(\text{H}_2\text{O}_3\text{PCH}_2)_2\text{N}-$ group and the use of this new linker in the synthesis of metal phosphonosulfonates. Thus the linker molecule $(\text{CH}_3\text{PO}_3\text{H}_2)_2\text{NCH}_2\text{C}_6\text{H}_4\text{SO}_3\text{H}$ (H_5L) was successfully synthesized and a high-throughput investigation resulted in the four new coordination polymers $[\text{Mg}(\text{H}_3\text{L})(\text{H}_2\text{O})_2]\cdot\text{H}_2\text{O}$ (**1**), $[\text{Mg}_2(\text{HL})(\text{H}_2\text{O})_6]\cdot 2\text{H}_2\text{O}$ (**2**), $[\text{Ba}(\text{H}_3\text{L})(\text{H}_2\text{O})]\cdot\text{H}_2\text{O}$ (**3**) and $[\text{Pb}_2(\text{HL})]\cdot\text{H}_2\text{O}$ (**4**). The syntheses, crystal structures and full characterization of these compounds are presented in detail.

2. Experimental

2.1 Materials and methods

All metal salts and solvents were used as received.

High-throughput powder X-ray diffraction (PXRD) patterns were measured in transmission geometry using $\text{Cu-K}\alpha_1$ ($\lambda = 1.54056 \text{ \AA}$, Mythen detector) radiation and employing a Stoe Stadi P Combi diffractometer equipped with a motorized XY stage. PXRD patterns used for in-depth analysis were recorded on a Stoe Stadi P diffractometer in transmission geometry using $\text{Cu-K}\alpha_1$ ($\lambda = 1.54056 \text{ \AA}$, Mythen detector) radiation. Conventional, in-house single-crystal X-ray diffraction (SCXRD) data were recorded with a Bruker APEX-II CCD diffractometer using $\text{Mo-K}\alpha$ radiation ($\lambda = 0.71073 \text{ \AA}$) or a Bruker D8 Venture equipped with a PHOTON 100 CPAD detector, using $\text{Mo-K}\alpha$ radiation.

Synchrotron SCXRD data were obtained at BioMAX, Max4 synchrotron, Lund.

Variable temperature (VT) PXRD measurements were recorded on a Stoe Stadi P Combi diffractometer ($\text{Cu-K}\alpha_1$ radiation, $\lambda = 1.54056 \text{ \AA}$, Mythen detector) equipped with a capillary furnace. For the measurements, the samples were transferred into 0.5 mm quartz capillaries and heated up in steps of 10 K between 25 and 500 °C and measured for 5 minutes each.

Thermogravimetric analyses were carried out with a Netzsch STA-409CD analyser under air stream with a flow rate of 75 ml min^{-1} and a heating rate of 4 K min^{-1} . NMR spectra were recorded on a Bruker Avance III spectrometer and IR spectra on a Bruker ALPHA-P A220/D-01 Fourier transform infrared (FTIR) spectrometer equipped with an attenuated total reflection (ATR) unit. Elemental analyses were carried out using a Euro EA 3000 analyser.

For the sorption measurements, the sample was activated for 16 hours at 120 °C under reduced pressure (10^{-2} kPa). The H_2O sorption experiment was carried out at 298 K. The stabi-

lity of the sample during the sorption experiment was confirmed by PXRD measurements.

2.2 Synthetic procedures

2.2.1 Synthesis of H_5L . The linker $(\text{H}_2\text{O}_3\text{PCH}_2)_2\text{N}-\text{CH}_2\text{C}_6\text{H}_4\text{SO}_3\text{H}$ was synthesized in a two-step reaction. In the first step, benzylamine (240 ml, 2.196 mol) was added dropwise to conc. H_2SO_4 (240 ml) under ice cooling within 1 h. After letting the mixture warm up to room temperature, 720 ml fuming sulphuric acid (30%) was added slowly. The mixture was heated up and stirred for two hours at 100 °C. Filtration gave 114.63 g of 4-sulfo-benzylamine, yield: 33.4%.

In the second step, 4-sulfo-benzylamine (114.63 g, 612.3 mmol) was dissolved in 925 ml of 5.2 M hydrochloric acid and subsequently, 72 g phosphonic acid (882 mmol, 3 eq.) was added. The resulting mixture was heated to reflux and formaldehyde (130 ml 37% aqueous solution, 1.61 mol, 5 eq.) was added dropwise over two hours. The solution was kept at reflux for 72 hours and the solvent was removed under reduced pressure. The resulting honey-textured product was repeatedly refluxed in $10 \times 150 \text{ ml}$ of acetone, which resulted in a grey powder. The crude product was stirred in 0.5 l of ethanol to give a white powder of H_5L (210.42 g, 91%).

^1H NMR (400 MHz, D_2O , TMS, 300 K): $\delta = 7.74$ (d, 2H, Ar-H), 7.57 (d, 2H, Ar-H), 4.64 (s, 2H, Ar- CH_2 -N), 3.35 (d, 4H, N- CH_2 -P) ppm.

Elemental analysis: calcd (%): C 28.61, H 4.03, N 3.73, S 8.55; found (%): C 28.55, H 4.13, N 3.61, S 8.29.

2.2.2 High-throughput investigation, discovery of the title compounds. High-throughput (HT) syntheses were carried out using a custom made 24-multiclave reactor system with a total volume of 2 ml and a filling volume of 1 ml as described previously.¹² Starting materials, molar ratios, solvent compositions and various counter ions of the metal salts were investigated. A complete overview of the experiments and the discovery of the title compounds is given in Tables S1 and S2.†

2.2.3 Synthesis scale-up of the title compounds. Scale-up of reaction conditions optimized by HT methods by a factor of 20 was easily accomplished. First the linker H_5L was introduced into a 30 ml autoclave as a powder. Subsequently water, ethanol, base and a solution of the respective metal salt were added in the given order. The reactor was closed and heated up to 150 °C for six hours, kept at 150 °C for 24 hours and cooled down to room temperature within twelve hours. The obtained products were filtered off and dried at room temperature. Exact amounts, stoichiometry and yields are given in Table 1.

Elemental analysis for **1** ($[\text{Mg}(\text{H}_3\text{L})(\text{H}_2\text{O})_2]\cdot\text{H}_2\text{O}$): calcd (%): C 23.94, H 4.24, N 3.10, S 7.10; found (%): C 23.94, H 4.17, N 3.12, S 7.71.

Elemental analysis for **2** ($[\text{Mg}_2(\text{HL})(\text{H}_2\text{O})_6]\cdot 2\text{H}_2\text{O}$): calcd (%): C 19.17, H 4.83, N 2.48, S 5.69; found (%): C 17.48, H 4.90, N 2.11, S 4.88.

Elemental analysis for **3** ($[\text{Ba}(\text{H}_3\text{L})(\text{H}_2\text{O})]\cdot\text{H}_2\text{O}$): calcd (%): C 19.70, H 3.49, N 2.55, S 5.85; found (%): C 20.07, H 3.04, N 2.44, S 5.71.

Table 1 Overview of the optimized synthesis conditions for the title compounds. The yield given in the last column is based on the linker

Compound	Metal source	M [mg]	M [ml]	Ratio metal	Linker [mg]	H ₂ O [ml]	EtOH [ml]	2 mol l ⁻¹ NaOH [ml]	Yield [%]
1 ([Mg(H ₃ L)(H ₂ O) ₂].H ₂ O)	MgCl ₂ ·6H ₂ O	1218	2	4	564	6.5	10	1.5	64.8
2 ([Mg ₂ (HL)(H ₂ O) ₆].2H ₂ O)	Mg(OAc) ₂ ·3H ₂ O	428	2	4	188	8	10	0	79
3 ([Ba(H ₃ L)(H ₂ O)]·H ₂ O)	BaCl ₂ ·2H ₂ O	244	2	2	188	8	10	0	41.1
4 ([Pb ₂ (HL)]·H ₂ O)	Pb(OAc) ₂ ·3H ₂ O	189	2	1	188	8	10	0	41.8

Elemental analysis for 4 ([Pb₂(HL)]·H₂O): calcd (%):C 13.45, H 1.63, N 1.74, S 3.99; found (%): C 13.70, H 1.82, N 1.80, S 3.54.

2.3 Crystal structure determination

Compounds 1, 2 and 3 were obtained as single crystals suitable for conventional single-crystal X-ray diffraction (SCXRD). The single crystal structures were solved using the program SHELXT¹³ and refined with SHELXL¹⁴ using Olex2¹⁵ as GUI. Title compound 4 formed dendritic crystals with very small dagger-shaped crystallites. Thus, data sets were acquired at the BioMAX beamline at Max4. The crystals endured severe radiation damage during the experiments, losing high angle diffraction (<1 Å) very fast and all diffraction after approximately one minute in the beam. The disordered nature of the crystals and the radiation damage gave very noisy data, but the structure could nevertheless be obtained by *ab initio* methods.

In the data sets of the Mg-based compounds 1 and 2, H-atoms could unequivocally be observed in the Fourier map and were subsequently refined. While in 1, all H-atoms were refined freely, during the structure refinement of 2 the H-atoms connected to the aromatic ring and free water molecules had to be added *via* AFIX instructions and refined using a riding model, the other H-atoms were refined using restraints. In 3 and 4, the H-atoms could not be localized at all from the Fourier map due to the influence of Ba and Pb ions as heavy scatterers. H-atoms connected to carbon were added *via* AFIX instructions and refined using a riding model.

3. Results and discussion

3.1 Synthesis

3.1.1 Synthesis of H₅L, (H₂O₃PCH₂)₂N-CH₂C₆H₄SO₃H. The new linker molecule H₅L was obtained in a two-step reaction as shown in Fig. 1. The first step, the sulfonation, was carried out according to Hubbuch *et al.* starting from benzylamine.¹⁶ For the second step, the phosphonomethylation, the procedure first described by Moedritzer and Irani¹⁷ was adapted with modified stoichiometry. The reported work-up procedure based on precipitation of the product upon addition of hot ethanol did not change the honey-like texture of H₅L. Thus, a different work-up procedure had to be evaluated, where repeated refluxing in acetone proved to be sufficient for converting the product into a solid powder. Further impurities were removed by stirring the powder in ethanol. NMR spectra (Fig. S12†) as well as CHNS analysis confirmed chemical purity.

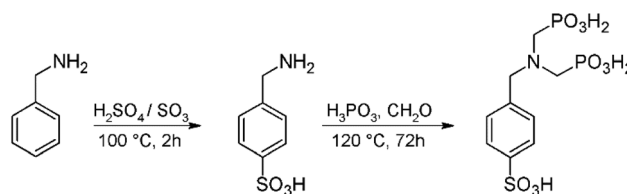


Fig. 1 Reaction scheme for the synthesis of H₅L, starting from benzylamine.

3.2 Synthesis of the coordination polymers

All metal phosphonosulfonates were synthesized under solvothermal reaction conditions employing a water/ethanol mixture as solvent. A high-throughput (HT) screening experiment using 20 different divalent metal salts with ionic radii varying between 0.72 and 1.47 Å was carried out in order to discover new CPs. A list of all metal salts and the exact synthesis parameters are given in section S2 in the ESI.† The use of ethanol as a co-solvent proved mandatory for obtaining crystalline reaction products and coordination polymers containing Mg²⁺, Ba²⁺ and Pb²⁺ ions were obtained. For the formation of 1, the concentration of the reactants had to be increased by a factor of three in order to obtain enough material for a full characterization.

The use of the different magnesium salts, *i.e.* MgCl₂·6H₂O and Mg(OAc)₂·4H₂O resulted in the formation of 1 and 2, respectively. To investigate the influence of the addition of acid or base on the formation of either 1 or 2, a systematic acid/base-screening was carried out. Synthetic details and results are summarized in Fig. S5.† Starting with MgCl₂·6H₂O as the metal source and adding NaOH (2 mol l⁻¹), the formation of 2 was observed, while the use of Mg(OAc)₂·3H₂O and adding HCl (2 mol l⁻¹) results in the formation of 1.

3.3 Crystal structures

Since all four compounds were obtained as single crystalline materials, their crystal structures were determined by single-crystal X-ray diffraction. Crystallographic details are given in Table 2.

Compound 1, [Mg(H₃L)(H₂O)₂].H₂O, exhibits the lowest degree of linker connectivity in all of the presented compounds, which is reflected in the IBU and the connection pattern of the linker. The asymmetric unit (Fig. S7†) contains one Mg²⁺ cation, three water molecules and a threefold protonated linker molecule. Isolated MgO₆ polyhedra are observed

Table 2 Crystallographic data of the title compounds

	1 ([Mg(H ₃ L)(H ₂ O) ₂]·H ₂ O)	2 ([Mg ₂ (HL)(H ₂ O) ₆]·2H ₂ O)	3 ([Ba(H ₃ L)(H ₂ O)]·H ₂ O)	4 ([Pb ₂ (HL)]·H ₂ O)
Sum formula	MgC ₉ H ₁₉ NO ₁₂ P ₂ S	Mg ₂ C ₉ H ₂₇ NO ₁₇ P ₂ S	BaC ₉ H ₁₇ NO ₁₁ P ₂ S	Pb ₂ C ₉ H ₁₁ NO ₉ P ₂ S
Crystal system	Monoclinic	Monoclinic	Orthorhombic	Monoclinic
λ [Å]	0.71073	0.71073	0.71073	0.72932
a [Å]	7.654(2)	18.8531(8)	15.569(3)	5.3434(1)
b [Å]	8.098(2)	5.3729(2)	24.683(5)	23.6346(3)
c [Å]	26.554(5)	23.791(1)	8.749(2)	13.1707(2)
α [°]	90	90	90	90
β [°]	90.64(3)	113.180(1)	90	91.839(1)
γ [°]	90	90	90	90
Space group	$P2_1/c$	$P2_1/n$	$Ama2$	$P2_1/c$
Tot., uniq. data, R_{int}	24123, 3752, 4.25	25674, 5014, 5.28	20223, 4303, 17.17	2337, 2337, 38.56
R_1 , wR_2 [$I > 2\sigma(I)$]	3.22, 8.61	5.36, 14.74	6.6, 18.5	16.8, 38.7
Observed data [$I > 2\sigma(I)$]	3489	3763	3882	1362
GOF	1.053	1.025	1.089	1.603

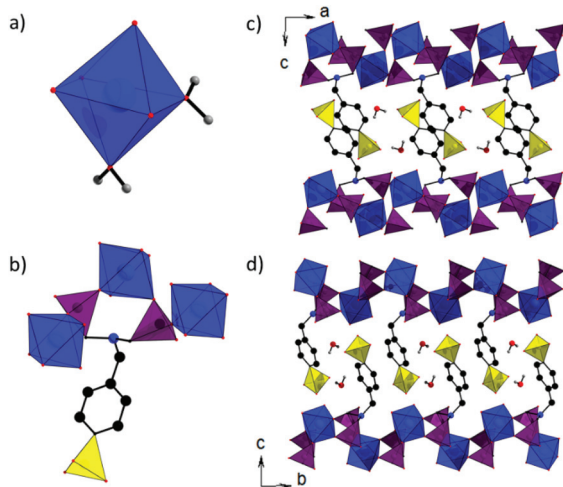


Fig. 2 Crystal structure of [Mg(H₃L)(H₂O)₂]·H₂O (1), (a) coordination environment of Mg²⁺-ions, (b) connectivity of the linker molecule, and two-dimensional network of 1 (c) along [010], (d) along [100]. General colour scheme: C (black), O (red), N (blue), P and P–O-tetrahedra (violet), S and S–O-tetrahedra (yellow), Mg (light blue) and Mg–O-octahedra (blue). Hydrogen atoms were omitted for clarity.

with oxygen atoms from two coordinating water molecules and four oxygen atoms of two H₃L²⁻ ions (Fig. 2). Each linker molecule connects three Mg²⁺ cations in a [2,110] fashion, according to the Harris notation.⁵ The third water molecule of the asymmetric unit is located between the layers forming several H-bonds (Fig. 8c and Table S4[†]). The remaining three acidic protons of the linker could be unequivocally localized from the Fourier map and were successfully refined. Zwitterions are present in the structure with –PO₃H⁻, –SO₃⁻ and ammonium groups. Extensive hydrogen bonding (Fig. 8c and Table S4) leads to a supramolecular 3D-structure.

Compound 2 features a slightly higher degree of linker connectivity and M–O condensation (Fig. 3). The asymmetric unit consists of two Mg²⁺ cations, six coordinating water molecules and a monoprotonated linker molecule (Fig. S8[†]). One linker connects five Mg²⁺ cations *via* the phosphonate groups coordinating in a [3,210] and a [3,111] fashion according to the

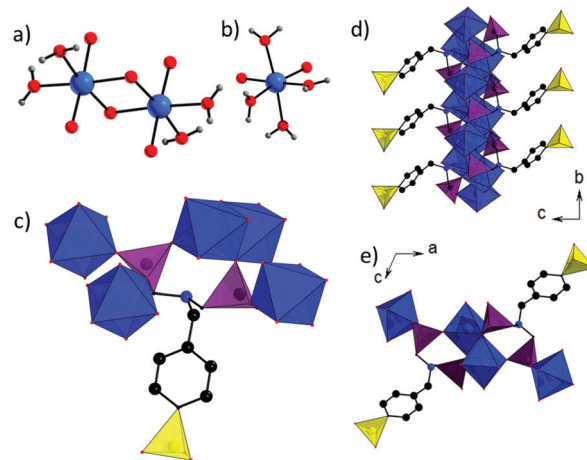


Fig. 3 Crystal structure of [Mg₂(HL)(H₂O)₆]·2H₂O (2), (a) coordination environment of Mg1, (b) coordination environment of Mg2, (c) coordination mode of the linker molecule; and one-dimensional structure of 2, (d) view along [100], (e) view along [010]. General colour scheme: C (black), O (red), N (blue), P and P–O-tetrahedra (violet), S and S–O-tetrahedra (yellow), Mg (light blue) and Mg–O-polyhedra (blue). Hydrogen atoms were omitted for clarity.

Harris notation,⁵ while the sulfonate group does not coordinate. The acidic proton could be located from the Fourier map and was successfully refined. It is connected to the nitrogen atom of the linker and it is involved in hydrogen bonding (Table S6[†]). In addition to the six coordinating water molecules, electron density in the Fourier map indicated the presence of additional water molecules. The non-coordinating water molecules are localized through hydrogen bonds and their presence is confirmed by the excellent agreement with the analytical data (sections 3.7 and S4[†]). Extended hydrogen bonding (Table S6[†]) leads to the formation of a 3D supramolecular structure.

In contrast, the crystal structure of compound 3, [Ba(H₃L)(H₂O)]·H₂O, shows a clear increase in condensation in the IBU and linker connectivity and thus does not resemble the interdigitated structural motif found in 1 and 2. This is due to the fact that the dimensionality of the IBU is increased and chains

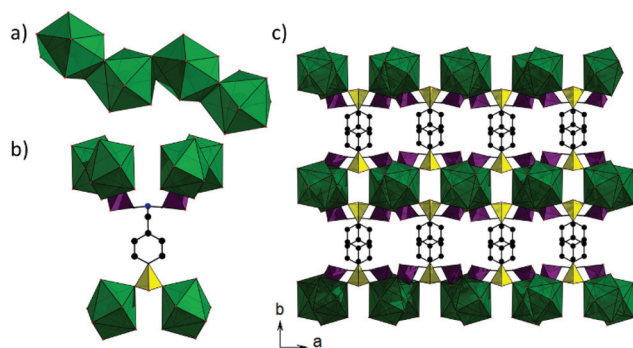


Fig. 4 Crystal structure of $[\text{Ba}(\text{H}_3\text{L})(\text{H}_2\text{O})]\cdot\text{H}_2\text{O}$ (**3**), (a) chain of edge-sharing BaO_9 -polyhedra, (b) coordination mode of the linker molecule, (c) three-dimensional network of **3**, view along $[001]$. General colour scheme: C (black), O (red), N (blue), P and P–O-tetrahedra (violet), S and S–O-tetrahedra (yellow), Ba and Ba–O-polyhedra (green). Hydrogen atoms were omitted for clarity.

of interconnected BaO_9 polyhedra are formed (Fig. 4). The asymmetric unit consists of one Ba atom, two oxygen atoms assigned to water molecules and two linker molecules on special positions (Fig. S9[†]). The Ba centre is coordinated by nine oxygen atoms, forming a monocapped square antiprism and edge-sharing of the BaO_9 polyhedra leads to zigzag-chains along $[001]$. This fact, combined with a coordinating sulfonate group, leads to the formation of a three-dimensional coordination polymer. The presence of hydrogen phosphonate groups is indicated by a P–O bond length of 1.551(10) Å which is in excellent agreement with the P–O bond lengths found for the P–OH groups in **1** (1.589(1) Å and 1.569(1) Å). The hydrogen phosphonate and sulfonate groups coordinate in a $[2,110]$ fashion, according to the Harris notation.⁵ Thus, each linker molecule connects six Ba^{2+} cations in total and is only twofold deprotonated. The third remaining proton is bonded to the nitrogen atom, thus forming a zwitterionic molecule.

Compound **4**, $[\text{Pb}_2(\text{HL})]\cdot\text{H}_2\text{O}$, exhibits similar structural features as **3**. In Fig. 5, similarities such as a one-dimensional chain of M–O-polyhedra and the coordination of the sulfonate group to the metal ion is shown. Yet, there are still differences regarding the structural motif found in **4**. The asymmetric unit is composed of two Pb^{2+} cations and one linker molecule. The Pb1 atom is coordinated by seven oxygen atoms in a distorted pentagonal bipyramidal fashion, while Pb2 is coordinated by five oxygen atoms and exhibits a distorted square-pyramidal coordination environment. The polyhedra of Pb1 and Pb2 are linked by edge-sharing to dimers, which are further connected *via* corner-sharing into chains along $[001]$. These chains are linked by phosphonate and sulfonate groups to layers which are further interconnected into a 3D framework by the organic part of the linker molecules. The increase in linker connectivity is reflected in the coordination of the two phosphonate and the sulfonate groups ($[4,211]$, $[3,211]$ and $[4,211]$, respectively, according to the Harris notation).⁵ The compound exhibits a stereochemically active electron pair pointing into the pore. Due to the presence of lead as a heavy scatterer, no

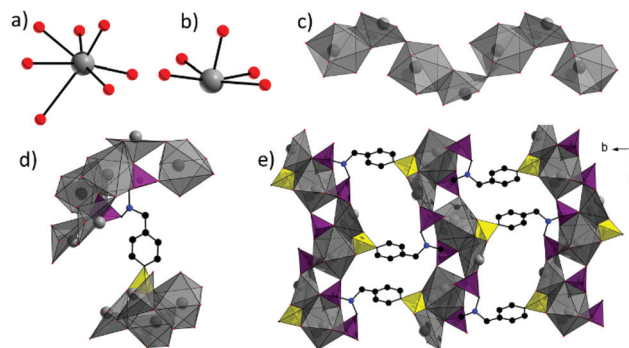


Fig. 5 Crystal structure of $[\text{Pb}_2(\text{HL})]\cdot\text{H}_2\text{O}$ (**4**), (a) coordination environment of Pb1, (b) coordination environment of Pb2, (c) chain of edge- and corner-sharing Pb–O-polyhedra along $[001]$, (d) coordination mode of the linker molecule, (e) three-dimensional network of **4**. General colour scheme: C (black), O (red), N (blue), P and P–O-tetrahedra (violet), S and S–O-tetrahedra (yellow), Pb and Pb–O-polyhedra (grey). Hydrogen atoms were omitted for clarity.

hydrogen atoms could be located from the Fourier map and thus they were placed on idealized positions and refined using a riding model. In order to achieve charge balance, the linker must be monoprotonated. Based on the observed bond length and the coordinating properties of the linker we conclude that the acidic proton is probably located on the nitrogen atom as observed in the other title compounds.

3.4 Structure discussion

Several similarities between the crystal structures can be observed. First, similarities between both Mg-based compounds (**1** and **2**) will be discussed, followed by the heavy metal-containing compounds (**3** and **4**); subsequently, the section will be concluded with a comparison to the structures already reported in the literature.

In all four compounds, zwitterionic linker molecules are found due to the deprotonation of the $-\text{SO}_3\text{H}$ group, a variable degree of deprotonation of the $-\text{PO}_3\text{H}_2$ groups, and the protonation of the tertiary amine.

Both **1** and **2** contain octahedrally surrounded Mg^{2+} cations with a minimum of two water molecules in their coordination environment. While only isolated MgO_6 polyhedra are observed in **1**, an IBU with higher degree of condensation, *i.e.* dimeric Mg_2O_{10} units are found in **2**. Both compounds exhibit a similar structural motif, layers with interdigitated aromatic cores and non-coordinating sulfonate groups. This results in a 2D-layered structure for **1** and a 1D-chain structure for **2**. The high amount of crystal water in the coordination sphere of Mg2 in **2** leads to a lower dimensionality, since it prevents the linker molecule from connecting the chains further.

The increase in ionic radius from 0.72 (Mg^{2+}) to 1.23 (Ba^{2+}) and 1.47 Å (Pb^{2+}) leads to an increase in the coordination number in **3** and **4** and thus a more variable coordination environment. One-dimensional chains of edge-/corner-sharing M–O polyhedra are observed in **3** and **4** and the higher degree of condensation of the IBU in combination with coordinating

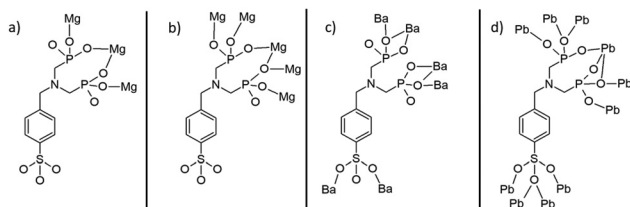


Fig. 6 Coordination modes of the linker molecules in the four title compounds, which reflects the increase in connectivity. (a) $[\text{Mg}(\text{H}_3\text{L})(\text{H}_2\text{O})_2] \cdot 2\text{H}_2\text{O}$ (**1**), (b) $[\text{Mg}_2(\text{HL})(\text{H}_2\text{O})_6] \cdot 2\text{H}_2\text{O}$ (**2**), (c) $[\text{Ba}(\text{H}_3\text{L})(\text{H}_2\text{O})] \cdot \text{H}_2\text{O}$ (**3**), (d) $[\text{Pb}_2(\text{HL})] \cdot \text{H}_2\text{O}$ (**4**).

sulfonate groups (Fig. 6) results in the formation of three-dimensional open framework structures with one-dimensional channel systems.

As previously stated, the dominant structural motif found in compounds containing amino bismethylenephosphonate groups are inorganic layers comprised of metal–oxygen–clus-

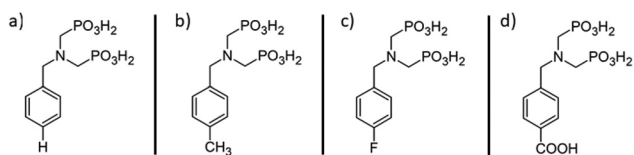


Fig. 7 Linker molecules of similar geometries and containing $(\text{H}_2\text{O}_3\text{PCH}_2)_2\text{N}-$ groups, which were employed in previous studies.^{19,20}

ters and phosphonate groups (motif A, Fig. 8, top left). The organic part of the linker molecules, the phenyl ring, is located between the layers, which leads to interdigitation.¹⁸ The crystal structure of **1** fits nicely into this pattern and the presence of the $-\text{SO}_3^-$ groups results in the formation of hydrogen bonds between the layers. The second motif (motif B, Fig. 8, top right) can be found in **2** but instead of 2D inorganic layers, interdigitated 1D-chains are formed. Due to the presence of sulfonate groups, coordinating water molecules and water of crystallisation, **1** and **2** exhibit an extensive network of hydrogen bonds. There are a few linker molecules of similar geometry (Fig. 7) that have also been used for the synthesis of coordination polymers. Interestingly, their crystal structures can be categorized according to the two motifs observed in the title compounds **1** and **2**. Details are given in the ESI, Table S12.†

Regarding the structure of **3** and **4**, the sulfonate group now takes part in the coordination of metal ions. This results in a 3D network structure. To the best of our knowledge, comparable structural motifs are not known to this date. Although there are several reports of a coordinating carboxylate group, the crystal structures arising thereof are best to be described as 2D-layered.¹⁹

3.5 Hirshfeld surface analysis

Hirshfeld surface analysis is a powerful tool for studying intermolecular interactions between molecules in crystalline solids, resolving various interatomic distances in a single picture.

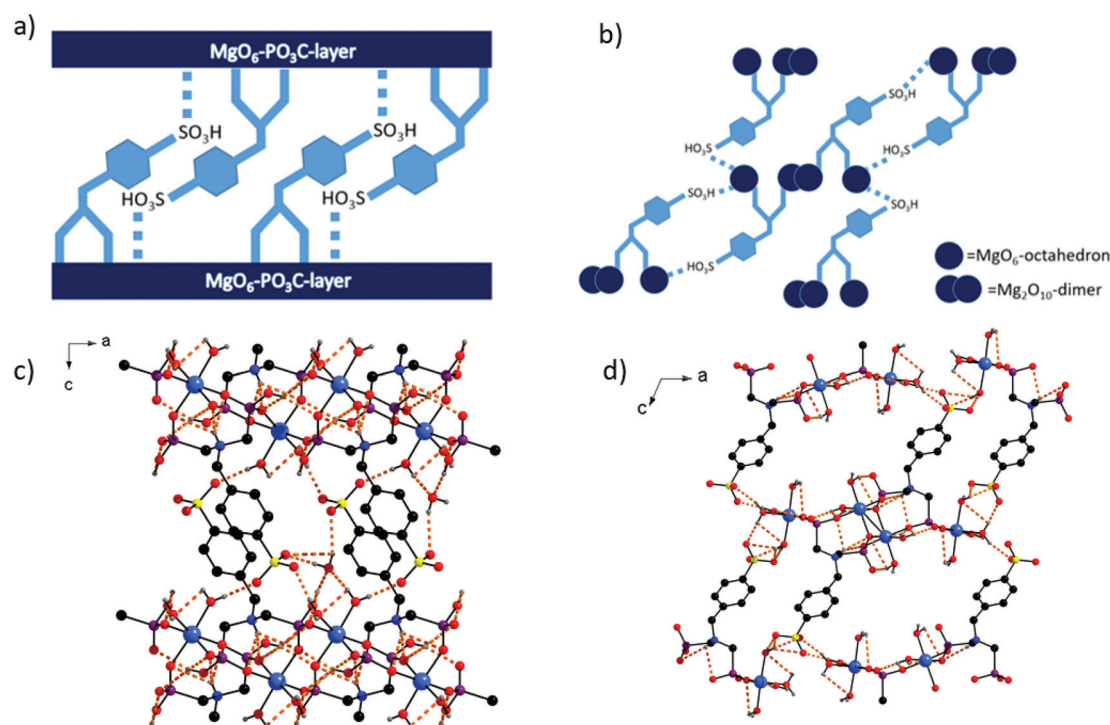


Fig. 8 Detailed insight into the structures of the Mg-based compounds (hydrogen bonds are represented through dashed lines), (a) simplified 2D-layered motif of **1** (motif A), (b) simplified 1D-layered chain-like motif of **2** (motif B), (c) network of hydrogen bonds in **1**, (d) network of hydrogen bonds in **2**.

This allows for detailed studies of the interactions which lead to a certain crystal packing, such as van der Waals-interactions, hydrogen bonds and other types. In order to study the nature of interactions between the layers in **1** and the chains in **2** in more detail, we carried out a Hirshfeld surface analysis. The calculations were performed using the Crystal Explorer17 program²⁰ and Hirshfeld surfaces were mapped using the normalized contact distance d_{norm} which is calculated according to the equation:

$$d_{\text{norm}} = \frac{d_i - r_i^{\text{vdW}}}{r_i^{\text{vdW}}} + \frac{d_e - r_e^{\text{vdW}}}{r_e^{\text{vdW}}}$$

where d_{norm} is the normalized contact distance, derived from d_e (the nearest atom outside the Hirshfeld surface), d_i (the nearest atom inside the Hirshfeld surface) and their respective van der Waals (vdW) radii.²¹ The 3D surfaces were mapped for d_{norm} and are shown in Fig. 9 using the standard red-white-blue colour scheme. Contacts shorter than van der Waals-radii are encoded in red and are characteristic for hydrogen bonds and other types of internuclear interactions. Contacts longer than van der Waals interactions are encoded in blue. Close inspection of the Hirshfeld surfaces for **1** and **2** reveals that hydrogen bonding occurs at the sulfonic acid groups and the water molecules attached to the metal centres. This provides additional evidence for the extent of hydrogen bonding discussed in section 3.4.

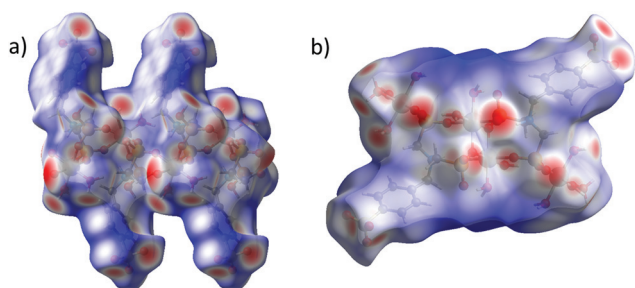


Fig. 9 (a) Hirshfeld surface of **1**, view along [100], (b) Hirshfeld surface of **2**, view along [010]. Contacts shorter than van der Waals contacts (*i.e.* covalent bonds and hydrogen bonds) are encoded in red, contacts longer than van der Waals interactions are encoded in blue. Details on the chosen structure sector are given in Fig. S16.†

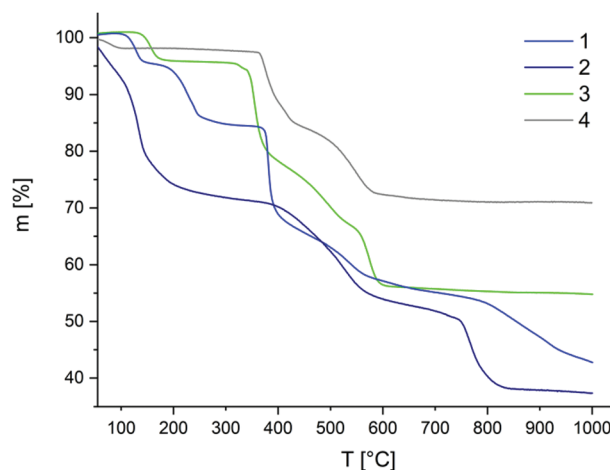


Fig. 11 TG curves of the title compounds under air.

3.6 Porosity and sorption

Since the crystal structure determination of **4** revealed the existence of pores, a sorption experiment was carried out. A detailed view of the pore, the water sorption isotherm and PXRD patterns of the sample before and after measurement are shown in Fig. 10. While compound **4** is non-porous to nitrogen at 77 K, a water uptake of 50 mg g⁻¹ at 298 K was detected which corresponds to 2.2 water molecules per formula unit. PXRD measurements confirmed the stability of the compounds towards H₂O de- and adsorption (Fig. 10c).

3.7 Thermal analysis

For all compounds, thermogravimetric analyses were carried out in order to verify the formulas deduced from the SCXRD experiments and to investigate the thermal stabilities between 30 and 1000 °C. The TG curves are shown in Fig. 11 and the assignment of the weight losses are given in Table 3. For each compound various weight losses are observed and the first one is related to the loss of water molecules while the second step corresponds to linker decomposition. For **1**, the loss of water is divided into two steps: the first step up to 150 °C corresponds to one water molecule per formula unit and can be assigned to the water of crystallisation, while the second step

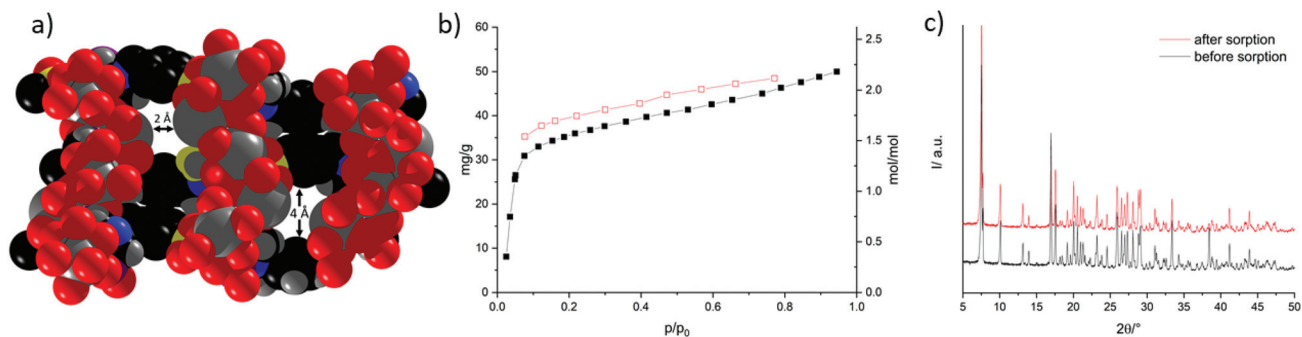


Fig. 10 (a) Pores in the structure of **4**, (b) water sorption curve of **4**, (c) PXRD pattern of **4** before and after sorption measurement.

Table 3 Overview of the TG analysis results

Compound	Mass loss H ₂ O			Mass loss linker decomposition			Residual mass	
	Obs. [%]	Calc. [%]	ΔT [°C]	Obs. [%]	Calc. [%]	ΔT [°C]	Obs. [%]	Calc. [%]
1 ([Mg(H ₃ L)(H ₂ O) ₂ ·H ₂ O])	13.7	11.97	25–370	43.56	47.67	370–1000	42.74	40.36
2 ([Mg ₂ (HL)(H ₂ O) ₆ ·2H ₂ O])	26.4	25.6	25–400	34.7	35	400–850	38.9	39.4
3 ([Ba(H ₃ L)(H ₂ O)]·H ₂ O)	5.8	6.5	25–185	40.4	39.61	310–600	53.8	53.82
4 ([Pb ₂ (HL)]·H ₂ O)	1.7	2.2	25–100	26.4	—	360–640	71	—

between 150 and 370 °C, presumably corresponds to the loss of the coordinating water molecules.

For each compound, the thermogravimetric analysis leads to a sum formula which is in good agreement with the results of the structure determination. A detailed comparison between calculated and measured values is given in Table 3. These results are further confirmed by elemental analyses.

3.8 IR-spectroscopy

The IR spectra of the title compounds and the linker molecule H₅L are shown in Fig. 12. The complete assignment of the bands is given in Table S11†²² and selected bands are discussed in this section. For the linker molecule, the strong and broad absorption bands between 3000 and 2000 cm⁻¹ can be assigned to the OH-stretching vibration of the sulfonic and phosphonic acid groups. In the structures of the CPs this group are partially or fully deprotonated, which leads to lower intensities or the absence of these bands in the IR spectra. Other broad adsorption bands between 3660 and 3100 cm⁻¹ can be assigned to the OH-valence vibration of the water molecules. An assignment of the bands to coordinating and non-coordinating water molecules is not possible since the water molecules are involved in hydrogen bonding (section S5†). Nevertheless, the intensity of these bands correlates with the amount of water molecules found within the structures *via* SCXRD and TG analysis. The weak bands at 1413 and 1431 cm⁻¹ can be assigned to the P-CH₂-R-groups (CH₂ defor-

mation vibration) and the strong band at 1647 cm⁻¹ observed for **1** and **2** corresponds to deformation vibrations of the water molecules. This band can be also be observed in the spectrum of **3**, but as expected from the composition with much smaller intensity.

The full assignment of the bands corresponding to the -SO₃ and -PO₃ groups is not straightforward, but trends are visible. The S-O and P-O stretching vibrations are anticipated between 1000 and 1300 cm⁻¹.²² In comparison to the bands observed in H₅L many shifts and changes in intensity are observed due to the coordination of these functional groups, the different degrees of protonation and their involvement in hydrogen bonding (section S5†). For compound **4** only one broad band is observed in this region which is in line with its crystal structure, *i.e.* the full deprotonation of the acid functions and the involvement of all oxygen atoms in the coordination of the Pb²⁺ ions (Fig. 6d).

4. Conclusions

The use of the new polyfunctional linker molecule (CH₂PO₃H₂)₂N-CH₂C₆H₄SO₃H led to the discovery of four new coordination polymers. While compounds **1** and **2** exhibit layered structures, for compound **3** and **4** 3D-framework structures are observed. The latter is a result of coordinating sulfonate groups, connecting two and four metal ions, respectively. Both framework compounds are potentially porous and permanent porosity was confirmed for **4** by water sorption measurements. In addition to the synthetic study and the crystal structure determinations presented herein, the full characterization of all title compounds is given.

The inclusion of a sulfonic acid group in linker molecules containing the (H₂O₃PCH₂)₂N- moiety can result in the formation of 3D CPs due to the coordination of the -SO₃ group. However, when the sulfonate group does not coordinate to the metal ions, the resulting structure resembles the layered, interdigitated motifs found for linker molecules containing the (H₂O₃PCH₂)₂N- moiety and -H, -CH₃, -F, -COOH functions.

Thus, the compounds presented herein are excellent examples for inorganic-organic hybrid materials with mixed functionalities. We have demonstrated that the use of these linker molecules can lead to the formation of free acid functionalities and porous materials. The anticipation of the structural motif remains a challenging task due to

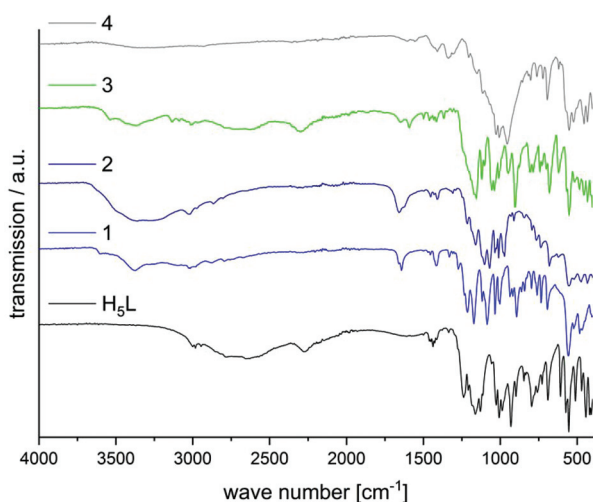


Fig. 12 IR spectra of H₅L and the title compounds.

the many unknown factors which control the formation of the final structure. Nevertheless, the reported title compounds will contribute to a better understanding of the chemistry of metal phosphonates and metal phosphonatosulfonates.

Conflicts of interest

There are no conflicts to declare.

Acknowledgements

The authors would like to thank Inke Jeß for the collection of single-crystal X-ray data and Prof. Christian Näther for helpful comments concerning the structure elucidations. E. S. G and A. K. I acknowledge support from the Swedish Foundation for Strategic Research. Financial support by the Deutsche Forschungsgemeinschaft (DFG, SPP 1928) is gratefully acknowledged.

References

- G. Yücesan, Y. Zorlu, M. Stricker and J. Beckmann, *Coord. Chem. Rev.*, 2018, **369**, 105–122.
- S. J. I. Shearan, N. Stock, F. Emmerling, J. Demel, P. A. Wright, K. D. Demadis, M. Vassaki, F. Costantino, R. Vivani, S. Sallard, I. Ruiz Salcedo, A. Cabeza and M. Taddei, *Crystals*, 2019, **9**, 270.
- M. Taddei, F. Costantino and R. Vivani, *Eur. J. Inorg. Chem.*, 2016, **2016**, 4300–4309.
- (a) B. Wang, T. Rhauderwiek, A. K. Inge, H. Xu, T. Yang, Z. Huang, N. Stock and X. Zou, *Chem. – Eur. J.*, 2018, **24**, 17429–17433; (b) P. Ramaswamy, N. E. Wong, B. S. Gelfand and G. K. H. Shimizu, *J. Am. Chem. Soc.*, 2015, **137**, 7640–7643; (c) J. M. Taylor, R. Vaidhyanathan, S. S. Iremonger and G. K. H. Shimizu, *J. Am. Chem. Soc.*, 2012, **134**, 14338–14340.
- A. Clearfield and K. Demadis, *Metal Phosphonate Chemistry. From Synthesis to Applications*, Royal Society of Chemistry, 2012.
- (a) E. Armakola, R. M. P. Colodrero, M. Bazaga-García, I. R. Salcedo, D. Choquesillo-Lazarte, A. Cabeza, M. V. Kirillova, A. M. Kirillov and K. D. Demadis, *Inorg. Chem.*, 2018, **57**, 10656–10666; (b) K. D. Demadis, E. Armakola, K. E. Papathanasiou, G. Mezei and A. M. Kirillov, *Cryst. Growth Des.*, 2014, **14**, 5234–5243; (c) K. D. Demadis, A. Panera, Z. Anagnostou, D. Varouhas, A. M. Kirillov and I. Císařová, *Cryst. Growth Des.*, 2013, **13**, 4480–4489.
- (a) Y. Zorlu, D. Erbahar, A. Çetinkaya, A. Bulut, T. S. Erkal, A. O. Yazaydin, J. Beckmann and G. Yücesan, *Chem. Commun.*, 2019, **55**, 3053–3056; (b) M. D. Allendorf, C. A. Bauer, R. K. Bhakta and R. J. T. Houk, *Chem. Soc. Rev.*, 2009, **38**, 1330–1352; (c) M. Casciola, U. Costantino, A. Peraio and T. Rega, *Solid State Ionics*, 1995, **77**, 229–233; (d) G. Alberti, *Solid State Ionics*, 1996, **84**, 97–104; (e) R. M. P. Colodrero, P. Olivera-Pastor, E. R. Losilla, D. Hernández-Alonso, M. A. G. Aranda, L. Leon-Reina, J. Rius, K. D. Demadis, B. Moreau, D. Villemin, M. Palomino, F. Rey and A. Cabeza, *Inorg. Chem.*, 2012, **51**, 7689–7698; (f) J. M. Taylor, K. W. Dawson and G. K. H. Shimizu, *J. Am. Chem. Soc.*, 2013, **135**, 1193–1196.
- G. Alberti, U. Costantino, F. Marmottini, R. Vivani and P. Zappelli, *Angew. Chem., Int. Ed. Engl.*, 1993, **32**, 1357–1359.
- K. Adil, Y. Belmabkhout, R. S. Pillai, A. Cadiou, P. M. Bhatt, A. H. Assen, G. Maurin and M. Eddaoudi, *Chem. Soc. Rev.*, 2017, **46**, 3402–3430.
- (a) W.-Q. Kan, J.-F. Ma, Y.-Y. Liu, J. Yang and B. Liu, *CrystEngComm*, 2012, **14**, 2268; (b) Q. Yue, J. Yang, G.-H. Li, G.-D. Li and J.-S. Chen, *Inorg. Chem.*, 2006, **45**, 4431–4439; (c) K. D. Demadis, Z. Anagnostou, A. Panera, G. Mezei, M. V. Kirillova and A. M. Kirillov, *RSC Adv.*, 2017, **7**, 17788–17799; (d) N. Hermer and N. Stock, *Dalton Trans.*, 2015, **44**, 3720–3723; (e) T. Rhauderwiek, H. Zhao, P. Hirschle, M. Döblinger, B. Bueken, H. Reinsch, D. de Vos, S. Wuttke, U. Kolb and N. Stock, *Chem. Sci.*, 2018, **9**, 5467–5478.
- (a) R. M. P. Colodrero, G. K. Angeli, M. Bazaga-Garcia, P. Olivera-Pastor, D. Villemin, E. R. Losilla, E. Q. Martos, G. B. Hix, M. A. G. Aranda, K. D. Demadis and A. Cabeza, *Inorg. Chem.*, 2013, **52**, 8770–8783; (b) M. Feyand, C. F. Seidler, C. Deiter, A. Rothkirch, A. Lieb, M. Wark and N. Stock, *Dalton Trans.*, 2013, **42**, 8761–8770; (c) M. Taddei, F. Costantino, A. Ienco, A. Comotti, P. V. Dau and S. M. Cohen, *Chem. Commun.*, 2013, **49**, 1315–1317.
- N. Stock, *Microporous Mesoporous Mater.*, 2010, **129**, 287–295.
- G. M. Sheldrick, *Acta Crystallogr., Sect. A: Found. Adv.*, 2015, **71**, 3–8.
- G. M. Sheldrick, *Acta Crystallogr., Sect. C: Struct. Chem.*, 2015, **71**, 3–8.
- O. V. Dolomanov, L. J. Bourhis, R. J. Gildea, J. A. K. Howard and H. Puschmann, *J. Appl. Crystallogr.*, 2009, **42**, 339–341.
- A. Hubbuch, R. Bindewald, J. Föhles, V. K. Naithani and H. Zahn, *Angew. Chem.*, 1980, **92**, 394–395.
- K. Moedritzer and R. R. Irani, *J. Org. Chem.*, 1966, **31**, 1603–1607.
- (a) Y.-Q. Guo, S.-F. Tang, B.-P. Yang and J.-G. Mao, *J. Solid State Chem.*, 2008, **181**, 2713–2718; (b) Z.-M. Sun, J.-G. Mao and Z.-C. Dong, *Polyhedron*, 2005, **24**, 571–577; (c) Z.-M. Sun, J.-G. Mao, Y.-Q. Sun, H.-Y. Zeng and A. Clearfield, *New J. Chem.*, 2003, **27**, 1326; (d) Z.-M. Sun, J.-G. Mao, B.-P. Yang and S.-M. Ying, *Solid State Sci.*, 2004, **6**, 295–300; (e) Z.-M. Sun, B.-P. Yang, Y.-Q. Sun, J.-G. Mao and A. Clearfield, *J. Solid State Chem.*, 2003, **176**, 62–68; (f) R. Vivani, F. Costantino, M. Nocchetti and G. D. Gatta, *J. Solid State Chem.*, 2004, **177**, 4013–4022; (g) R. Zeng, X. Fu, Y. Sui, X. Yang, M. Sun and J. Chen, *J. Organomet. Chem.*, 2008, **693**, 2666–2672; (h) Y.-Y. Zhu, Z.-G. Sun,

- F. Tong, Z.-M. Liu, C.-Y. Huang, W.-N. Wang, C.-Q. Jiao, C.-L. Wang, C. Li and K. Chen, *Dalton Trans.*, 2011, **40**, 5584–5590; (i) Z.-M. Sun, J.-G. Mao and Z.-C. Dong, *Polyhedron*, 2005, **24**, 571–577; (j) Z.-M. Sun, B.-P. Yang, Y.-Q. Sun, J.-G. Mao and A. Clearfield, *J. Solid State Chem.*, 2003, **176**, 62–68; (k) H. Xu, H. Zhou, L. Feng, Q. Wang, R. Chen, W. Huang and X. Wu, *Dalton Trans.*, 2018, **47**, 11226–11238.
- 19 (a) S. Bauer, T. Bein and N. Stock, *Inorg. Chem.*, 2005, **44**, 5882–5889; (b) S. Bauer, J. Marrot, T. Devic, G. Férey and N. Stock, *Inorg. Chem.*, 2007, **46**, 9998–10002; (c) H. Luo, C. Ma, C.-Q. Jiao, Z.-G. Sun, T. Sun, M.-X. Ma, Y.-Y. Zhu, W.-Z. Li, M.-L. Wang and X.-W. Zhang, *New J. Chem.*, 2015, **39**, 6611–6622; (d) H. Luo, Y.-Y. Zhu, Z.-G. Sun, C.-Q. Jiao, G.-N. Zhang, T. Sun, M.-X. Ma and W.-Z. Li, *RSC Adv.*, 2014, **4**, 49892–49899; (e) J.-L. Song and J.-G. Mao, *J. Mol. Struct.*, 2005, **740**, 181–186; (f) S.-F. Tang, J.-L. Song and J.-G. Mao, *Eur. J. Inorg. Chem.*, 2006, **2006**, 2011–2019; (g) W. Zhou, J. Zhang, Z.-G. Sun, Y.-Y. Zhu, C.-Q. Jiao, S.-P. Shi, L.-L. Dai, T. Sun, W.-Z. Li, M.-X. Ma and H. Luo, *Inorg. Chem. Commun.*, 2014, **47**, 37–41; (h) W. Zhou, Y.-Y. Zhu, C.-Q. Jiao, Z.-G. Sun, S.-P. Shi, L.-L. Dai, T. Sun, W.-Z. Li, M.-X. Ma and H. Luo, *CrystEngComm*, 2014, **16**, 1174.
- 20 M. J. Turner, J. J. McKinnon, S. K. Wolff, D. J. Grimwood, P. R. Spackman, D. Jayatilaka and M. A. Spackman, *CrystalExplorer17*, 2017.
- 21 M. A. Spackman and D. Jayatilaka, *CrystEngComm*, 2009, **11**, 19–32.
- 22 George Socrates, *Infrared and Raman Characteristic Frequencies: Tables and Charts*, Wiley, 2004.